Journal of The Electrochemical Society

OPEN ACCESS

Imaging the Surface of a Polycrystalline Electrodeposited Cu Film in Real Time Using In Situ High-Speed AFM

To cite this article: Aswathi Koorikkat *et al* 2020 *J. Electrochem. Soc.* **167** 162510

View the article online for updates and enhancements.

You may also like

- A monolithic MEMS position sensor for closed-loop high-speed atomic force microscopy
N Hosseini, A P Nievergelt, J D Adams et al.

- Dynamic Observation of 2686 bp DNA–BAL 31 Nuclease Interaction with Single Molecule Level Using High-Speed Atomic Force Microscopy
Hiroaki Sugasawa, Yukihiro Sugiyama, Takashi Morii et al.

- Mapping real-time images of high-speed AFM using multitouch control
D M Carberry, L Picco, P G Dunton et al.

This content was downloaded from IP address 217.39.82.213 on 06/07/2023 at 16:49

Journal of The Electrochemical Society, 2020 **167** 162510

Imaging the Surface of a Polycrystalline Electrodeposited Cu Film in Real Time Using In Situ High-Speed AFM

Aswathi Koorikkat,[1] Oliver Payton,[1] Loren Picco,[2] and Walther Schwarzacher[1,*,z]

[1]*H.H Wills Physics Laboratory, University of Bristol, Bristol BS8 1TL, United Kingdom*
[2]*Virginia Commonwealth University, Richmond, Virginia 23284, United States of America*

We studied the surface evolution of polycrystalline Cu films electrodeposited from an organic additive-free acid sulphate electrolyte on to a gold microelectrode using a high-speed Atomic Force Microscope (HS-AFM) which images an area of 2 × 2 μm at 2 frames per second and a resolution of 1000 × 1000 pixels. The ability to acquire data at this rate opens even fast growth processes to in situ investigation. Real-time images from a film deposited at ~0.5 nm s^{-1} revealed many interesting phenomena, most significantly highly non-uniform grain growth rates with several examples of grains showing accelerated growth compared to their neighbours. Grain overgrowth was also observed in different regions of the sample. Surface roughness scaling and slope analysis provided evidence for structural coarsening of the film and an increase in the mean slope θ with increasing film thickness t. We show how both grain overgrowth and an increase in θ can contribute to the coarsening of the surface structure as deposition proceeds.
© 2020 The Electrochemical Society ("ECS"). Published on behalf of ECS by IOP Publishing Limited. This is an open access article distributed under the terms of the Creative Commons Attribution 4.0 License (CC BY, http://creativecommons.org/licenses/by/4.0/), which permits unrestricted reuse of the work in any medium, provided the original work is properly cited. [DOI: 10.1149/1945-7111/abd0cb]

Manuscript submitted October 6, 2020; revised manuscript received November 20, 2020. Published December 18, 2020.

Supplementary material for this article is available online

Electrodeposited polycrystalline metal films have numerous applications as conducting interconnects in the electronics and semiconductor industries[1] or for purposes of decoration or corrosion protection.[2] Processes such as grain growth and grain boundary motion that affect the microstructure and morphology of a polycrystalline thin film play an important role in determining its mechanical[3] or electrical properties.[4] To optimize these it is crucial to understand how the microstructure and surface morphology evolve during growth.

Various studies have looked at how factors like temperature,[5] anion adsorption[6] and stress[7] influence the growth of polycrystalline electrodeposited films. However, the vast majority of studies have involved characterization carried out post-growth, and very few studies have addressed the challenge of understanding surface structural evolution via experiments carried out in situ in real time. Such experiments are essential to obtain information on the dynamics of the processes involved.

To date some of the most useful data have come from in situ measurements of surface stress using the wafer curvature technique, which have provided evidence that adatom insertion into grain boundaries during growth causes compressive stress that is relieved when the growth is interrupted.[8] Other measurements have shown how grain coarsening affects the surface stress.[9] Although considerable insight has been gained from these investigations, they lack the spatial information that imaging techniques provide.

In situ scanning tunnelling microscopy is capable of providing extremely high resolution structural data at high rate[10,11] but has only rarely been applied to the growth of polycrystalline thin films, where it was limited to relatively slow deposition.[12] In situ atomic force microscopy can also deliver high-resolution images of electrochemical systems and this technique was used to image polycrystalline Zn films electrodeposited from an ionic liquid electrolyte with nm-scale resolution,[13] for example. However, although the Zn electrodeposition rate in this study was up to a few monolayers per second, deposition had to be interrupted for imaging, because of the relatively low speed of standard AFM: the authors reported a holding time of approximately 10 min per image. In contrast, researchers using one of the various HS-AFMs developed to date[14] are able to capture topographic images at rates up to 1,000 times faster than are possible with conventional AFMs. In pioneering work, Matsushima and co-workers used an intermittent contact mode HS-AFM to study Cu electrodeposition and dissolution on Au(100)[15] and Au (111).[16] However, these studies were restricted to very thin films grown on single-crystal substrates.

Here, we apply a contact mode HS-AFM during growth to study the later stages in the electrodeposition of a thin Cu film on a polycrystalline Au substrate. The working electrode was a microelectrode to ensure good mass transport despite the small volume of electrolyte used in the HS-AFM experiment. Scanning the same area of the film continuously during deposition made it possible to observe individual grains[a] at different stages of growth. We could identify phenomena that took place as the film thickness increased, such as neighbouring grains growing at very different rates and the overgrowth of one grain by another. These observations could be related to trends revealed by scaling and slope analysis. This is the first time that such high-resolution structural data has been obtained in situ in real time from a polycrystalline thin film grown at such a rapid rate (up to ~0.5 nm s^{-1}). In future, such studies should lead to a greatly enhanced understanding of the microstructural evolution of polycrystalline electrodeposited films.

Methods

The working electrode used was prepared by evaporating gold onto a glass substrate. A microelectrode of diameter 30 μm was patterned on to the substrate using positive resist and UV photolithography. The copper films were deposited from an organic additive-free 0.01 M $CuSO_4$ + 0.1 M H_2SO_4 electrolyte. The reference and counter electrode was a Cu strip of purity 99.99% and the deposition was carried out potentiostatically at −200 mV for a deposition time of 120 s. At this potential, deposition is expected to be under mixed diffusion-kinetic control (see supplementary material, Fig. S6 is available online at stacks.iop.org/JES/167/162510/mmedia). The electrolyte was de-aerated using nitrogen for 30 min prior to the experiment.

Figure 1 shows a schematic of the experimental arrangement. The substrate was mounted on a specially designed sample holder which is capable of holding small quantities of electrolyte without spilling while the HS-AFM is scanning. The HS-AFM (Bristol Nano Dynamics Ltd. Mk2 contact-mode HS-AFM) scanned the surface using a 1 Hz slow scan raster pattern and a 1 kHz fast scan frequency. We collected data at 2 million pixels per second to generate two 1 mega pixel images per second. Measurements used cantilever "C" on a commercially available AFM probe chip (Bruker MSNL). These probes combine a Si tip and Si nitride cantilever.

*Electrochemical Society Active Member.
[z]E-mail: w.schwarzacher@bristol.ac.uk

[a]The grains referred to in this paper are volumes associated with particular topographic features rather than volumes that necessarily have a single crystal lattice orientation (crystallites). Each "grain" could consist of several crystallites with orientations related by twinning, for example.

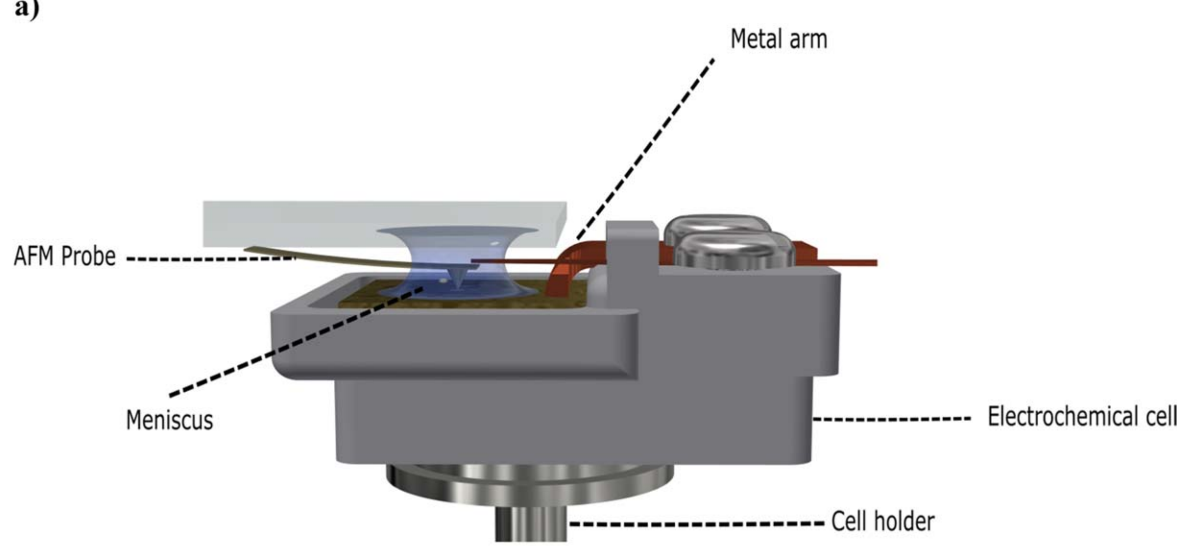

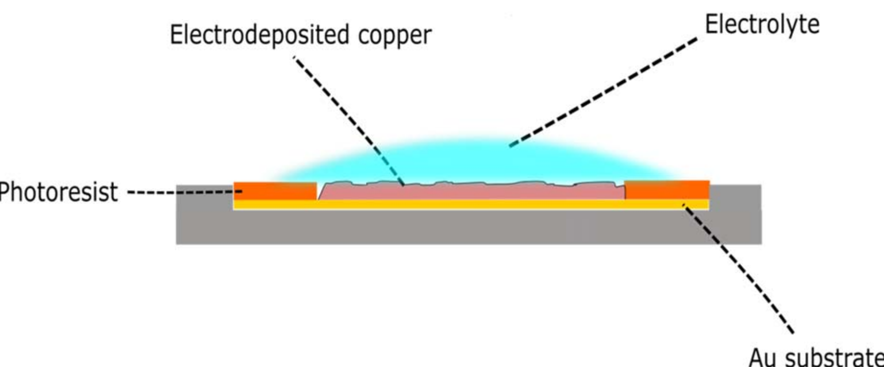

Figure 1. (a) 3D view of the electrochemical cell (b) schematic cross-sectional view of the patterned substrate for in situ AFM.

The HS-AFM scans a fixed area of the substrate while the deposition takes place. This produces a high resolution video of the deposition process from the onset of deposition to the endpoint, where the grains have grown to a significantly larger size. Each video frame is saved as an image consisting of a 1000×1000 array, where the row and column number define the position on the image and the corresponding array element gives the height at that point. Heights are given relative to the mean height. Images were analyzed using "Gwyddion"[17] as well as proprietary Bristol Nanodynamics software and our own code written in Python.

To describe the evolution of the overall film morphology quantitatively, we applied scaling analysis[18] whereby the topography of the growing film is characterized by a scale-dependent surface width $w(l)$:

$$w(l,\, t) \;=\; \sqrt{\langle (h - \langle h \rangle)^2 \rangle} \qquad [1]$$

where h is the height of the surface, l is the length scale over which w is measured and t is the film thickness, or deposition time in the case of constant growth rate. It has been shown that for real and model systems $w(l,\, t)$ often follows power laws of the form:

$$w(l,\, t) \;\propto\; l^H\, t^{\beta_{loc}} \text{ for } l \ll l_c \qquad [2a]$$

$$w(l,\, t) \;\propto\; t^{\beta + \beta_{loc}} \text{ for } l \gg l_c \qquad [2b]$$

H and β represent the Hurst exponent and growth exponent respectively. l_c is the cross-over length. When $\beta_{loc} > 0$ the scaling is referred to as anomalous, while $\beta_{loc} = 0$ refers to normal scaling, a special case of anomalous scaling.

To complement the scaling analysis, we also determined the local film slope θ, defined as the angle between the local surface normal and the normal to the film, as a function of position. θ is obtained by dividing an image into triangles formed by a point $(x_i,\, y_j,\, z_{i,j})$ and two of its neighbours, for example $(x_{i+1},\, y_j,\, z_{i+1,j})$ and $(x_i,\, y_{j+1},\, z_{i,j+1})$, then calculating the angle between the normal to this triangle and the film normal as described previously.[19]

Results

We grew and imaged a number of Cu films for this study but focus here on a film deposited for 120 s at an applied potential of −0.2 V for which the video is included in the supplementary

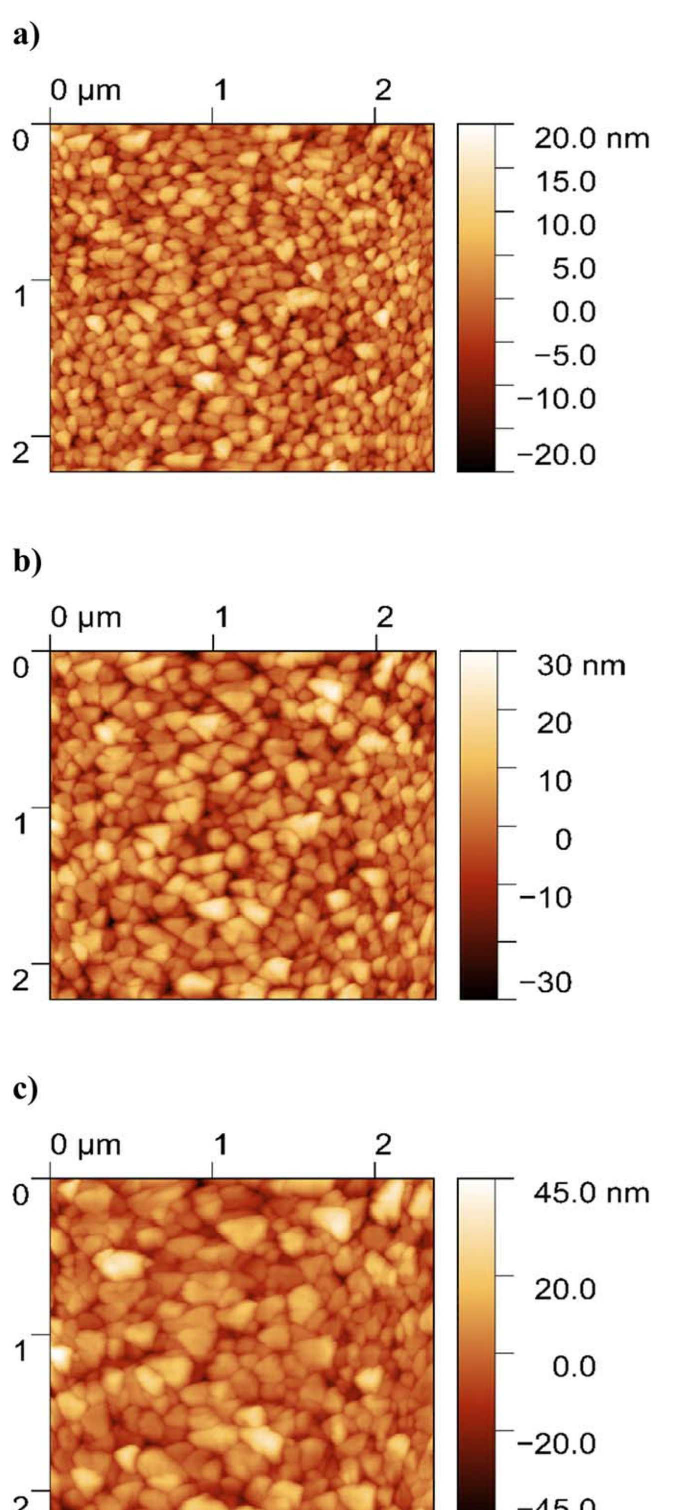

Figure 2. AFM images of the Cu film at different stages of growth: (a) $t \sim 24$ s; (b) $t \sim 68$ s; (c) $t \sim 119$ s.

material. The substrate was held at 0 V prior to the initiation of film growth in video frame 28. Video frames before 28 show the polycrystalline Au substrate. As deposition progresses, it is clear that the grains grow in size as shown in Fig. 2. A triangular bias to the grain shape visible from the start of the video is most likely due to tip convolution effects, but these effects do not prevent observation of the film structure coarsening during growth. There was also some sample drift during the experiment but we corrected for this

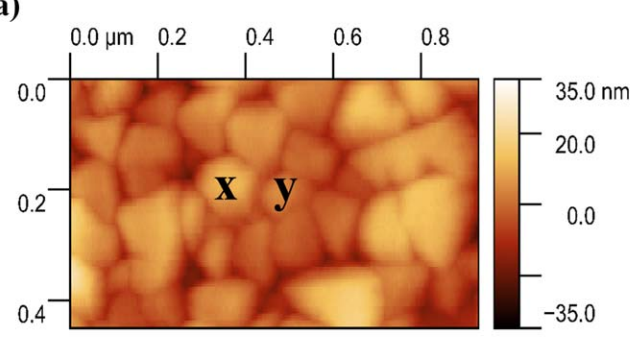

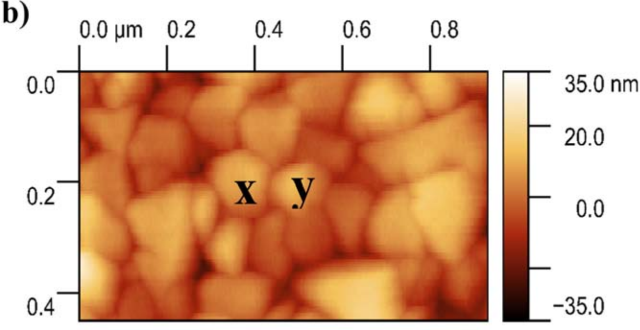

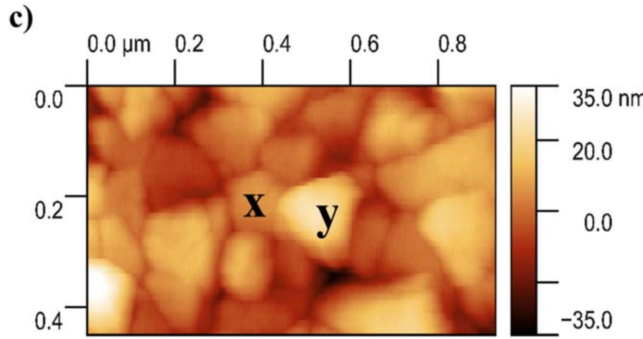

Figure 3. (a)–(c) High magnification images of a selected region of the Cu film at different stages of growth (a): $t \sim 68$ s; (b): $t \sim 77$ s; (c): $t \sim 101$ s illustrating the accelerated growth of the grain labelled "y". (d)–(f) Cross-sections of the grains marked "x" and "y" taken from the images (a)–(c).

using a customized Python programme to align features in successive video frames.

The growth rate for this film was $\sim 0.5 \text{ nm s}^{-1}$, estimated from HS-AFM images of a film grown under similar conditions that include the electrode edge and therefore enable direct determination of the film growth rate (see supplementary material, Fig. S1). Careful study of the video reveals a number of interesting features. Figure 3 shows a particularly clear example of a phenomenon that may be observed at a number of locations, namely the accelerated growth of a grain relative to its neighbours. From Figs. 3a–3c it is apparent that the grain labelled "y" grew significantly faster than its neighbours. Figures 3d–3f show corresponding cross-sections across grains "x" and "y". Initially the grain labelled "y" is similar in lateral extent to the neighbouring grain labelled "x", but its height is significantly lower (Fig. 3d). However, as deposition proceeds, its height overtakes that of x (Fig. 3e), and eventually exceeds it significantly (Fig. 3f). Further examples of accelerated local growth are presented in the supplementary material (Figs. S2 to S4).

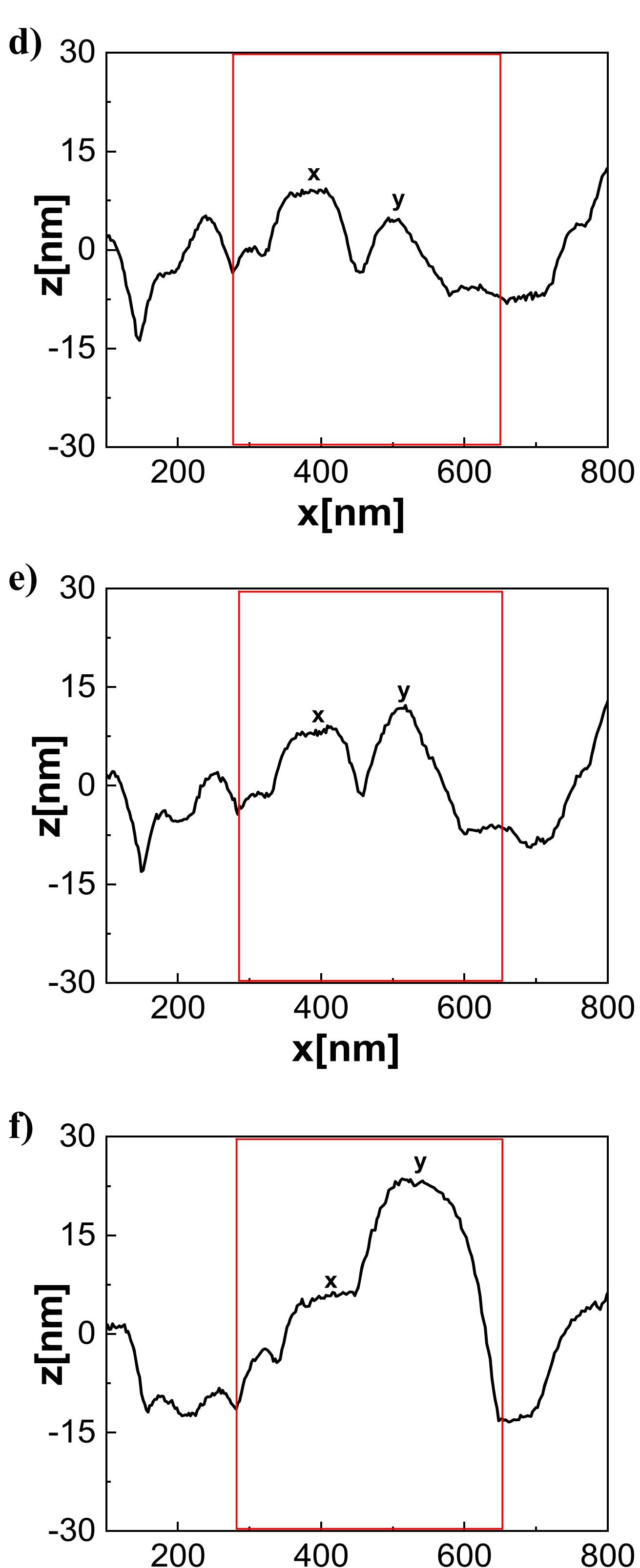

Figure 3. (Continued.)

Accelerated local growth starts and stops at different times for different grains.

Overgrowth of one grain by another is also observed as a consequence of non-uniform growth rates, including the example of Fig. 3. Note that as grain "y" overtakes its neighbours, it also partly overgrows them. Figure 4 is another clear example of overgrowth. Here, as deposition proceeds, the grain labelled "1" grows more rapidly than the smaller grain labelled "2". Grain "1" grows laterally over grain "2" (and other neighbours), partially engulfing it.

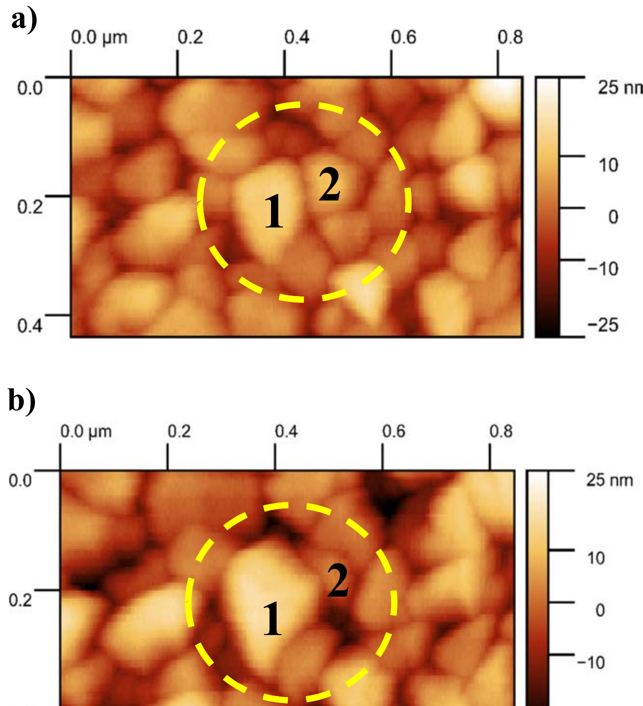

Figure 4. High magnification images illustrating overgrowth of the grain labelled "1" over the grain labelled "2" at different stages of growth (a) $t \sim 45$ s; (b) $t \sim 89$ s.

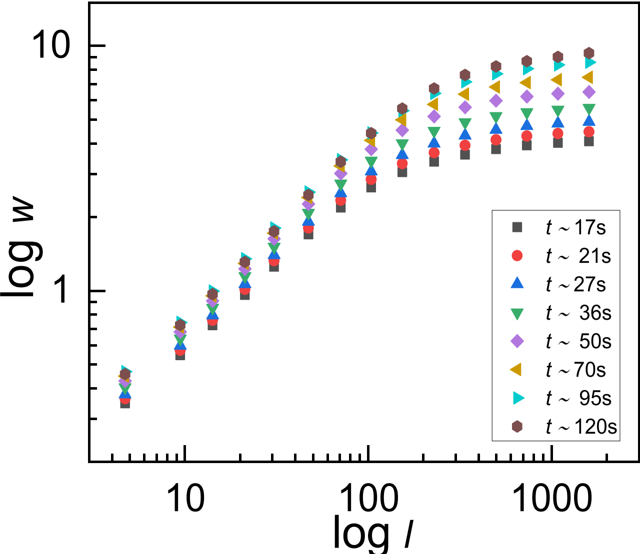

Figure 5. Logarithmic plot of surface width w vs the length scale l over which it is measured (see text for full definition of $w(l)$) at different film growth times t.

In addition to considering specific features of interest, it is useful to consider how global parameters that describe the topography of the film vary during growth. As an example, Fig. 5 presents surface roughness scaling data for the film of Figs. 2–4. The surface width w is calculated as a function of the length scale l over which it is

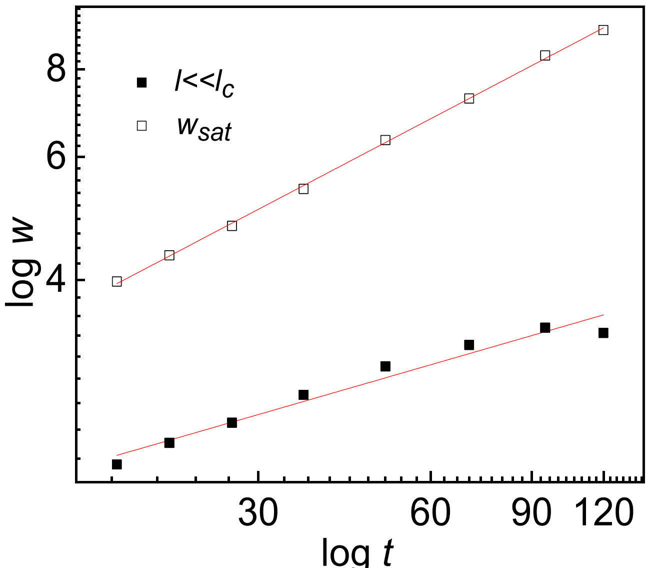

Figure 6. Logarithmic plots of w for $l \ll l_c$ ($l = 70$ nm) vs t and of w_{sat} vs t. The gradient of the latter gives $\beta + \beta_{loc} \approx 0.43$.

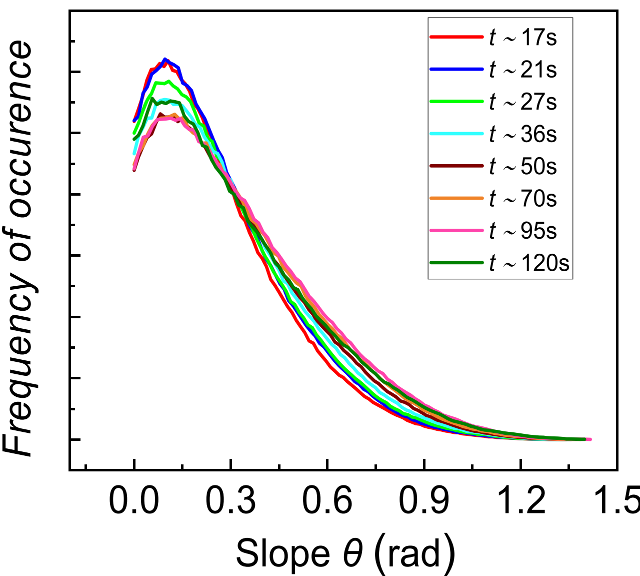

Figure 7. Plot showing the frequency of occurrence of a local slope θ (see text for a fuller description of θ) at different film growth times t.

measured as described in section 2. Different symbols in Fig. 5 correspond to different frames from the HS-AFM video and therefore to different deposition times t.

Each scaling curve in Fig. 5 may be divided into two regions, one for smaller values of l, where the gradient is positive, and one for larger values of l, where the roughness tends to a saturation value w_{sat}. The crossover between these regions corresponds to $l = l_c$, and from Eq. 2a, the gradient for $l \ll l_c$ is equal to H. In order to estimate values of w_{sat}, l_c and H consistently, each log-log plot in Fig. 5 was fitted using the equation[20,21]:

$$w(l) = w_{sat}(1 - \exp[-(l/l_c)^H]) \quad [3]$$

The mean value of H obtained in this way was 0.82. Both w for $l \ll l_c$ and w_{sat} increase with deposition time t (Fig. 6). The plot of $\log w_{sat}$ vs $\log t$ is linear, indicating that the power law relationship Eq. 2b holds with $\beta + \beta_{loc} \approx 0.43$. The plot of $\log w$ for $l \ll l_c$ vs

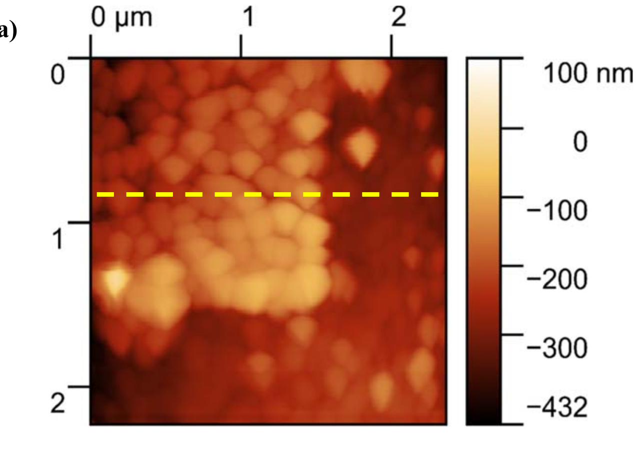

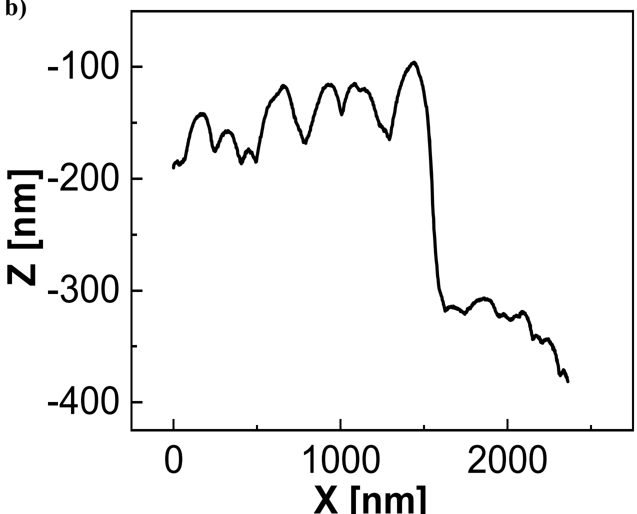

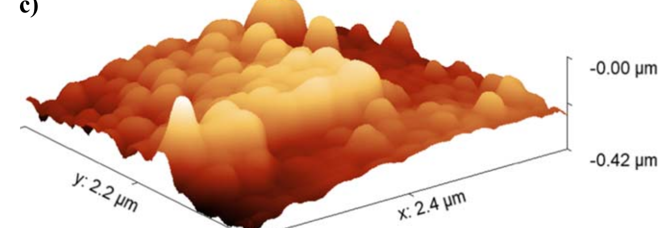

Figure 8. (a) A HS-AFM video frame recorded shortly after the scanning area was changed while growing a film under the same conditions as Figs. 2–4. The previous scanning area occupies the upper left part of the image; (b) Cross-section along the dashed line marked in (a); (c) The data of (a) shown in 3D.

$\log t$ is less obviously linear, but it is still clear that for small l, except at the final growth stages, $w(l)$ increases with t, which is inconsistent with normal scaling.[22] An increase in $w(l)$ with t for small l is a strong indicator that the local slope of the film is increasing.[19]

Figure 7 shows directly how the measured probability distribution for θ changes as the film thickness varies. It is interesting to note that although the mean θ does increase with t (see Table SI in the supplementary material) this mainly arises because of changes in the high θ "tail" rather than a shift in the maximum of the probability distribution to higher values of θ. However, a previous study which included much thicker films did show such a shift in the maximum of the probability distribution.[19]

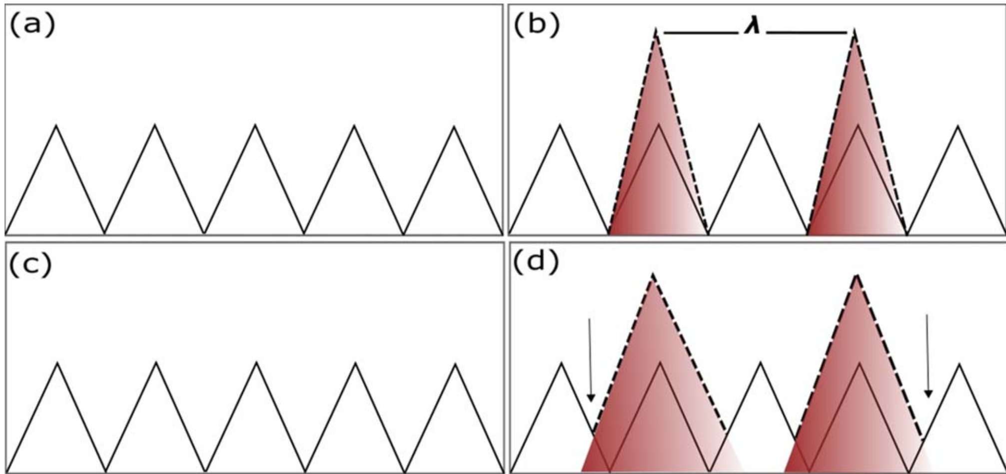

Figure 9. Schematics to show how grains growing at different rates lead to the surface structure coarsening in the absence (a)–(b) and presence (c)–(d) of grain overgrowth. The arrows in (d) point to the new apparent positions of the grain boundary at the sample surface. For an explanation of "λ" in (b), see text.

With the HS-AFM it is possible to move the imaging window while continuing to image in real-time. If the new imaging area and the old overlap, it is possible to see whether the imaging process itself affects the film growth. Figure 8a shows a frame recorded shortly after such a move was made while growing a film under the same conditions as Figs. 2–4. The previous scanning area occupies the upper left of the image Fig. 8a and appears brighter, corresponding to a greater height. The greater height of the previously scanned area is also obvious in the 3D image, Fig. 8c. The cross-section Fig. 8b shows that the transition between the two areas is abrupt, with a step in height of ∼200 nm between the peaks of adjacent grains.

Figure 8 shows clearly that film growth is more rapid where imaging takes place than elsewhere on the substrate. A similar effect has been observed previously and was attributed to the presence of a partially passivating oxygen adlayer on the Cu that could be disrupted by the AFM tip to accelerate growth.[23] Evidence for this mechanism came from the dependence of the observed enhanced deposition on tip-sample force, electrolyte pH and Cu crystallographic orientation. Interestingly, the enhanced deposition effect was also independent of dissolved oxygen content.[24] Further work is needed to determine whether the same mechanism is primarily responsible for the growth rate enhancement that we observe where imaging takes place, as it is possible that there could also be a contribution from forced convection caused by the tip movement. Stirring of the electrolyte by the tip would enhance mass transport, resulting in a higher local rate of deposition where the tip scans, and this is likely to be a more significant effect here than in conventional AFM experiments due to the much faster scan rate of the HS-AFM. However, the effects of forced convection will be less local than disruption of a partially passivating adlayer by the tip, so the abruptness of the transition between enhanced and non-enhanced deposition seen in Fig. 8 suggests that the latter is more important.

Discussion

Figure 2 clearly shows that the surface structure of our electrodeposited polycrystalline Cu film coarsens laterally during growth. Furthermore, the value of l_c determined by fitting the scaling data of Fig. 5 increases with time and deposit thickness (see supplementary material Fig. S5). Previous ex situ studies of polycrystalline Cu films electrodeposited from organic additive-free acid sulphate solutions have also shown qualitatively and through measurements of l_c that surface features become larger as the film thickness increases.[25] However, it hasn't been clear how this structural coarsening takes place.

Our observation of adjacent grains growing at different rates is significant because varying local growth rates provide a mechanism for structural coarsening. Different growth rates for different grains may or may not be accompanied by grain overgrowth, but either way they lead to coarsening of the surface structure. The no-overgrowth case is illustrated schematically in Figs. 9a–9b. Grains that grow faster than their neighbours dominate the topography so that their separation λ determines l_c rather than the individual grain size, as shown in Fig. 9b. Note that due to the constraints imposed by geometry, this type of coarsening is accompanied by an increase in the mean slope. In contrast, Figs. 9c–9d show an example of coarsening with grain overgrowth but no change in the mean slope. In practice, a combination of the mechanisms shown in Figs. 9a–9b and 9c–9d is observed. Cross-sections such as those of Fig. 3 show both overgrowth and an increase in the local slope: grain "y" overgrows its neighbours, and its slope (on the opposite side to grain "x") increases significantly from Figs. 3d to 3f. Figure 7 provides further evidence that the local slope increases. However, tip convolution effects could also affect the relative contributions of grain overgrowth and slope increases to the HS-AFM images—this requires further investigation.

Structural coarsening associated with non-uniform grain growth rates as shown in Fig. 9 is different to the structural coarsening predicted by the widely-studied van der Drift model,[26] since in the latter, structural coarsening is possible even when all exposed facets grow at a uniform rate. To understand the origin of the varying grain growth rates that we observe would require additional information beyond the surface topography. However, since our data shows that the film surface during growth does not consist of flat facets, it is probable that growth is under kinetic rather than thermodynamic control and that the microstructure plays a key role.

Electrodeposition is driven by the difference in electrochemical potential between a solvated ion in the bulk solution and a metal atom at a site where growth can take place (a half-crystal position[27] or kink site). The difference in electrochemical potential (overpotential) is distributed across the different stages of the process, including mass transport to the surface, electrochemical reduction of the ions, mass transport on the surface and adatom incorporation in the lattice. One grain can grow faster than another if it has a greater density of half-crystal sites, or if one of the other stages in the deposition process requires a lower overpotential locally to sustain a given rate. The latter is the case for diffusion limited growth, for example, where the transport overpotential is less at a protrusion than a hollow. However, in the present study, grains that start to grow rapidly do not appear to protrude relative to their neighbours—see e.g. grain "y" in Fig. 3. We therefore believe the most likely

explanation for the observed intermittent rapid growth is therefore a greater availability of growth sites, which in turn is a function of the grain orientation, topography and any defects present, i.e. of the microstructure. This remains true even when the availability of growth sites is limited by additives or partial passivation as could be the case here.[23] Possible candidates for microstructural features that favour rapid grain growth include the five-fold twin structures discussed by Pangarov and Velinov that incorporate a “seam” where the density of growth sites is likely be especially high.[28,29] Stacking fault structures with numerous steps could also contribute.[30]

Conclusions

We have conducted in situ HS-AFM measurements of an electrodeposited polycrystalline Cu film growing at a rate of $\sim 0.5\ \mathrm{nm\ s^{-1}}$ in order to understand how the morphology evolves during growth. The in situ electrochemical HS-AFM is extremely well-suited to this task, given its unique combination of a very high spatial resolution and exceptional time resolution for a scanning probe technique. By using a patterned microelectrode as substrate, it is possible to ensure adequate mass transport even with a small electrolyte volume, which enables the study of electrodeposition at a rate of several monolayers per second.

Our study of Cu electrodeposited from an additive-free acid sulphate electrolyte revealed interesting details of the growth process. In particular, it showed directly how variations in the local growth rate contribute to the coarsening of the film topography. We could image grain overgrowth directly. Furthermore, scaling analysis and the probability distribution for the local slope θ both show that the grain slope changes with time as the film grows. We also found that the AFM tip has a role in enhancing the local growth rate of the film. In future HS-AFM is likely to yield even more insight into polycrystalline film growth when combined with detailed post-growth microstructural characterization.

Acknowledgments

A. Koorikkat acknowledges a studentship supported by the Sir Frederick Charles Frank Fund. O. D. Payton and L. Picco would like to acknowledge funding and support from the Royal Academy of Engineering.

ORCID

Aswathi Koorikkat https://orcid.org/0000-0002-7281-1764
Oliver Payton https://orcid.org/0000-0003-4515-0603
Loren Picco https://orcid.org/0000-0002-3758-0972
Walther Schwarzacher https://orcid.org/0000-0003-0451-0940

References

1. C. Andricacos, C. Uzoh, J. Dukovic, J. Horkans, and H. Deligianni, *IBM J. Res. and Dev.*, **42**, 567 (1998).
2. M. Schlesinger and M. Paunovic, *Modern Electroplating* (Wiley, New York) (2011).
3. C. V. Thompson and R. Carel, *J. Mech. Phys. Solids,*, **44**, 657 (1996).
4. G. Palasantzas, *Phy. Rev. B*, **58**, 9685 (1998).
5. Y. Gründer, N. M. Markovic, P. Thompson, and C. A. Lucas, *Surf. Sci.*, **631**, 123 (2015).
6. N. Vasiljevic, M. Wood, P. Heard, and W. Schwarzacher, *J. Electrochem. Soc.*, **157**, D193 (2010).
7. S. Hearne, S. Seel, J. Floro, C. Dyck, W. Fan, and S. Brueck, *J. Appl. Phys.*, **97**, 083530 (2005).
8. J. W. Shin and E. Chason, *Phys. Rev. Lett.*, **103**, 056102 (2009).
9. A. M. Engwall, Z. Rao, and E. Chason, *J. Electrochem. Soc.*, **164**, D828 (2017).
10. O. M. Magnussen, *Chem. Eur. J.*, **25**, 12865 (2019).
11. Y. I. Yanson and M. J. Rost, *Angew. Chem.*, **52**, 2454 (2013).
12. M. J. Rost, *Phys. Rev. Lett.*, **99**, 266101 (2007).
13. J. S. Keist, C. A. Orme, P. K. Wright, and J. W. Evans, *Electrochim. Acta*, **152**, 161 (2015).
14. O. D. Payton, L. Picco, and T. B. Scott, *Inter. Mater. Rev.*, **61**, 473 (2016).
15. T. Yoshioka, H. Matsushima, and M. Ueda, *Electrochem. Commun.*, **92**, 29 (2018).
16. T. Yoshioka, H. Matsushima, and M. Ueda, *Electrochim. Acta*, **302**, 422 (2019).
17. D. Nečas and P. Klapetek, *Cent. Eur. J. Phys.*, **10**, 181 (2012).
18. W. Schwarzacher, *J Condens. Matter Phys.*, **16**, R859 (2004).
19. L. Liu and W. Schwarzacher, *Electrochem. Commun.*, **29**, 52 (2013).
20. R. Cecchini, J. J. Mallett, and W. Schwarzacher, *Electrochem. Solid-State Lett.*, **6**, C103 (2003).
21. S. K. Sinha, E. B. Sirota, S. Garoff, and H. B. Stanley, *Phys. Rev. B*, **38**, 2297 (1988).
22. M. Lafouresse, P. Heard, and W. Schwarzacher, *Phys. Rev. Lett.*, **98**, 236101 (2007).
23. J. R. LaGraff and A. A. Gewirth, *J. Phys. Chem.*, **98**, 11246 (1994).
24. J. R. LaGraff and A. A. Gewirth, *J. Phys. Chem.*, **99**, 10009 (1995).
25. S. Huo and W. Schwarzacher, *Phys. Rev. Lett.*, **86**, 256 (2001).
26. A. van der Drift, *Philips Res. Rep.*, **22**, 267 (1967).
27. H. Gerischer, *Electrochim. Acta*, **2**, 1 (1960).
28. N. Pangarov and V. Velinov, *Electrochim. Acta*, **13**, 1641 (1968).
29. M. C. Lafouresse, Y. Fukunaka, T. Homma, S. Honjo, S. Kikuchi, and W. Schwarzacher, *Electrochem. Solid-State Lett.*, **14**, D77 (2011).
30. C.-C. Lin and C.-C. Hu, *J. Electrochem. Soc.*, **167**, 082505 (2020).